Large-Eddy Simulation of the Turbulent Flow in the Downstream Region of a Backward-Facing Step

A. Silveira Neto,[1] D. Grand,[1] O. Metais,[2] and M. Lesieur[2]

[1]*Commissariat à l'Energie Atomique, Direction des Réacteurs Nucléaires, Centre d'Etudes Nucléaires de Grenoble, Service des Transferts Thermiques–Laboratoire de Physique Modélisation et Logiciels (LPML), 85 X, 38041 Grenoble CEDEX, France*

[2]*Institut de Mécanique de Grenoble, BP 53 X, 38041 Grenoble CEDEX, France*

(Received 5 November 1990)

A numerical simulation of a complex turbulent shear flow using large-eddy simulation techniques is carried out. The filtered Navier-Stokes equations are solved with a finite-volume method. The subgrid model is a local adaptation to the physical space of isotropic spectral eddy-viscosity models. The statistics of the mean field are in good agreement with the experimental data available, corresponding to a low step. Calculations in a high-step case show that the eddy structure of the flow presents striking analogies with the plane shear layers, with large billows shed behind the step, and longitudinal hairpin vortices strained between these billows.

PACS numbers: 47.25.Ae, 47.25.Ei, 47.25.Gk

Most of the natural flows are turbulent. Although an exact modeling of turbulence is still an unresolved challenge, methods for engineering computations had to be developed. They are based on the existing knowledge of turbulence, and are limited by the constraint of available computational resources. For many years, the only practical approach was through the time-averaged equations at one point and the use of semiempirical turbulence models.

An alternative approach is the development of large-eddy simulations,[1,2] in which the temporal evolution of the large-scale structures is obtained directly from the numerical simulation. The motions of wavelengths smaller than the computational grid (subgrid scales) have to be represented by a proper statistical model.

In this Letter, we report on the results of a three-dimensional (3D) large-eddy simulation of a complex inhomogeneous shear flow: the flow downstream of a backward-facing step in a plane channel (Fig. 1). The results of the numerical simulation are first compared to the experiment of Eaton and Johnston.[3] In this experiment, the aspect ratio defined as the height W of the channel downstream of the step over the height of the step H is 2.5. The Reynolds number based upon the upstream bulk velocity U_0 and H is 38000. These are the velocity and length scales used afterwards in the presentation of the results.

A first study[4] has been published for a two-dimensional simulation of this flow. Here we present three-dimensional simulations using a subgrid-scale model which allows us to consider high-Reynolds-number flows.

We solve the Navier-Stokes equations for an incompressible fluid, relating the filtered velocity vector u_i and pressure p:

$$\partial_i u_i = 0 , \tag{1}$$

$$\partial_t u_i + \partial_j (u_i u_j) = -\rho^{-1} \partial_i p + \nu \nabla^2 u_i + \partial_j \tau_{ij} . \tag{2}$$

Here, τ_{ij} is the subgrid-stress tensor. The boundary condition at the inlet is $u_1 = U_0 + \xi$, where U_0 is the bulk velocity and ξ a white noise of amplitude $10^{-4} U_0$, modeling the residual turbulence within the upstream flow. In our calculations, in fact, the backward-facing-step flow is always unstable, even without the inlet noise. A similar behavior was obtained for the spatial mixing layer by Buell and Huerre.[5] These are two cases where instabilities which are convectively unstable become absolutely unstable numerically. Upper and lower boundaries are of the impermeable and no-slip type in order to represent the rigid walls. The extent of the computational domain in the spanwise direction is limited by computational resources. In order to reduce the perturbations caused by this limited extent, a symmetry condition is imposed on the lateral planes. At the outlet, the longitudinal gradients of flow variables are set equal to zero.

These transport equations are solved numerically with the aid of software used for 3D computations of industrial flows: the TRIO code, developed at Commissariat à l'Energie Atomique. The finite-volume version of the code derived from the SOLA method[6] is used hereafter, with a third-order discretization scheme for the convective terms (SMART scheme[7]).

The subgrid model is based on the gradient transport hypothesis:

$$\tau_{ij} = 2\nu_t S_{ij} - \tfrac{2}{3} K_s \delta_{ij} , \tag{3}$$

where $S_{ij} = \frac{1}{2} (\partial_i u_j + \partial_j u_i)$ is the local strain, δ_{ij} the unit tensor, and K_s the subgrid turbulent kinetic energy. The eddy viscosity ν_t is borrowed from Kraichnan's spectral eddy viscosity,[8] developed by Chollet and Lesieur[9] for isotropic turbulence: We start with a viscosity ν_t scaling

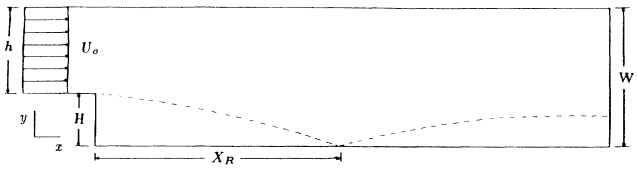

FIG. 1. Flow domain.

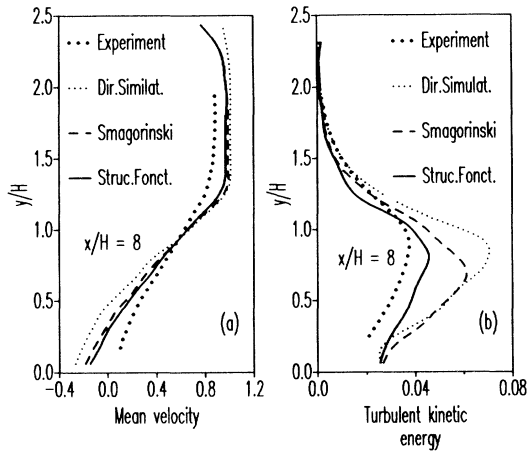

FIG. 2. (a) Transverse profile of the mean longitudinal velocity and (b) transverse profile of the turbulent kinetic energy at $x/H=8$ (coarse grid).

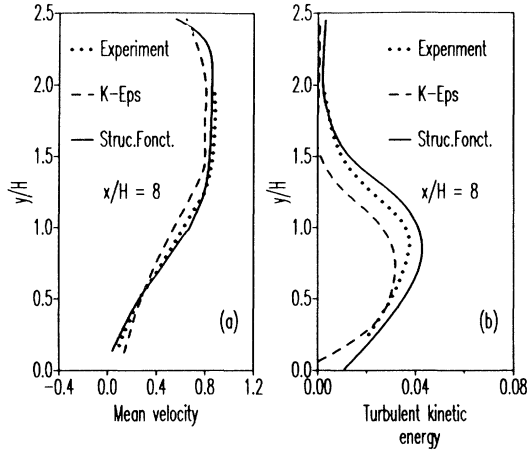

FIG. 3. (a) Transverse profile of the mean longitudinal velocity and (b) transverse profile of the turbulent kinetic energy at $x/H=8$ (finer grid).

on the kinetic-energy spectrum at the cutoff wave number k_c, with a simplified form given by

$$v_t(t)=v_t^+[E(k_c,t)/k_c]^{1/2}. \quad (4)$$

The constant $v_t^+=0.4$ is determined by the energy balance $\int_0^{k_c}2v_t k^2E(k,t)dk=\epsilon(t)$, where ϵ is the kinetic-energy flux along a Kolmogorov spectrum: $E(k)=C_k\epsilon^{2/3}k^{-5/3}$. It yields $v_t^+=\frac{2}{3}C_k^{-3/2}=0.4$ (with $C_k=1.4$).

A generalization of the model to highly intermittent and nonhomogeneous situations in physical space was proposed by Métais and Lesieur.[10] For a homogeneous and isotropic turbulence, they obtain the following result:

$$v_t(t)=0.04\Delta x[F_2(\Delta x,t)]^{1/2}, \quad (5)$$

where the quantity $F_2(r,t)$ is the second-order velocity structure function defined by

$$F_2(r,t)=\langle||\mathbf{u}(\mathbf{x}+\mathbf{r},t)-\mathbf{u}(\mathbf{x},t)||^2\rangle, \quad (6)$$

and the operator $\langle\cdot\rangle$ stands for an ensemble average, or may also be interpreted as a spatial average over the shell $r=||\mathbf{r}||$. The constant 0.04 in (5) is obtained with the aid of the relation (see Batchelor[11])

$$F_2(r,t)=4\int_0^\infty E(k,t)[1-\sin(kr)/kr]dk.$$

An approximation for $F_2(\Delta x,t)$ must be deduced from the filtered velocity, since the subgrid-scale field is unknown. Let $\bar{F}_2(\Delta x,t)$ be the corresponding structure function: Assuming that the energy spectrum follows Kolmogorov's law above the cutoff, it is found that

$$v_t(\mathbf{x},t)=0.06\Delta x[\bar{F}_2(\mathbf{x},\Delta x,t)]^{1/2}. \quad (7)$$

$\bar{F}_2(\mathbf{x},\Delta x,t)$ is calculated at each node and for each time step from the instantaneous flow. Since we are working on a regular grid of mesh Δx, the average is performed on the six points a distance Δx apart from the node $\mathbf{x}$ in the three directions of space. The subgrid model given by (7) will be called the structure-function model.

The first calculations using (7) were performed for $W/H=2.5$, on a coarse grid with, respectively, 91, 17, and 17 grid points in the longitudinal, transverse, and spanwise directions. Figures 2(a) and 2(b) show the transverse profiles of the mean longitudinal velocity and of the turbulent kinetic energy. The profiles are located in the reattachment region ($x/H=8$) in the middle of the channel. The turbulent kinetic energy, evaluated at each point by an integration over a time interval $400H/U_0$, consists of two parts: a contribution

$$\overline{u_i'u_i'}/2$$

corresponding to the fluctuations u_i' with respect to the time average $\bar{u}_i$ of the instantaneous filtered field u_i on the one hand, and a subgrid energy K_s on the other hand. The latter is estimated by a proper extrapolation of the local kinetic-energy spectrum, derived from the local structure function. Results are compared with a laboratory experiment[3] and with two other simulations using the same numerical code, one without any subgrid model and one using Smagorinsky's model:[12]

$$v_t(\mathbf{x},t)=(C_s\Delta)^2(2S_{ij}S_{ij})^{1/2}, \quad (8)$$

where $C_s=0.23$ and $\Delta=(\Delta_1\Delta_2\Delta_3)^{1/3}$, Δ_i being the grid spacing. Other numerical experiments on the channel flow[1] indicate that the turbulence quantities are insensitive to variations of C_s of the order of 20%. As for the structure-function model, we have not yet analyzed its sensitivity to variations of the constant arising in (7). Notice, however, that the numerical calculations presented below are lengthy (10 or 20 h per run on a CRAY2), and cannot be extensively repeated.

These results show that the eddy viscosity correspond-

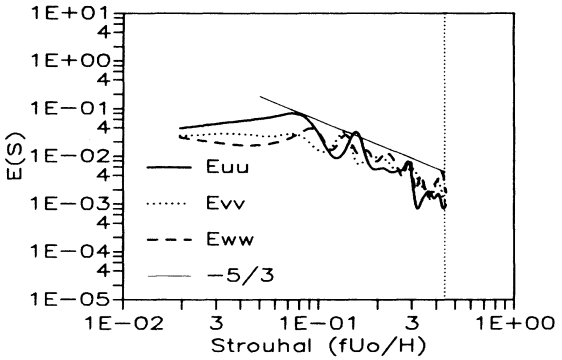

FIG. 4. Frequency spectra of the velocity fluctuations (the frequency f is normalized by the Strouhal number $S=fH/U_0$).

ing to the structure-function model gives a better agreement with the experiment as compared to Smagorinsky's formulation. The mean velocity profile [Fig. 2(a)] is less influenced by the subgrid-scale model.

The numerical simulation with the structure-function model was repeated on a finer grid ($200\times30\times30$). The results are shown in Fig. 3(a) and 3(b). The agreement with the laboratory experiment is significantly improved, particularly for the mean velocity profile. The maximum discrepancy between numerical and experimental results is less than 10% for the turbulent kinetic energy, within the range of the experimental error. In Figs. 3(a) and 3(b) are also shown the results given by the K-ϵ statistical model implemented in the TRIO code: The position of the peak of K is not well predicted, and neither is the mean velocity profile.

The large-eddy simulation also improves the prediction of the reattachment distance X_R/H, as shown by the following results: experiment[3], $X_R/H=7.8$; large-eddy simulation (fine grid), $X_R/H=8.1$; and K-ϵ model (grid-independent result), $X_R/H=6.2$.

The frequency spectra for the three velocity fluctuations u_i' are plotted in Fig. 4. They are measured in the region of reattached flow ($x/H=12$, $y/H=1$, and in the central region of the channel). They exhibit a well-defined $S^{-5/3}$ range ($S=fH/U_0$ is the Strouhal number, and f the time frequency) over one decade. The energy in the smaller scales is evenly distributed among the three components, indicating a trend towards isotropy. The distribution of energy in the larger scales is anisotropic, the streamwise component of velocity being the most energetic. The spectral peak of the turbulent intensity E_{uu} is found at a Strouhal number ($S=0.08$) comparable to Eaton and Johnston's value ($S=0.07$).

Visualizations of the instantaneous flow field at time $t=90H/U_0$ are shown in the next figures. Figure 5 displays the vortex structure: A plane sheet appears just downstream of the step (left-hand side of the figure). It oscillates, giving rise to large billows of spanwise vorticity. Streamwise vortices are stretched between the primary billows. Near the reattachment region, the presence of the wall introduces an extra source of stretching, leading to a high three dimensionalization of the structures.

FIG. 5. Vorticity contours at time $t=90H/U_0$: light gray, vorticity modulus $||\mathbf{w}||=3.5U_0/H$; dark gray, streamwise vorticity $w_x=2.5U_0/H$ (aspect ratio $W/H=2.5$).

Figure 6 shows a top view of the low-pressure surface corresponding to a fluctuation (with respect to the pressure at the outlet) $p'=-0.3U_0^2/\rho_0$. Three primary rolls are clearly visible. The closest to the step is roughly cylindrical, reflecting its quasi-two-dimensional character. The two other pressure tubes are highly three dimensional. They are linked by two streamwise tubes corresponding to the secondary vortices.

In the above case of a low step, the vortex structures forming downstream are strongly influenced by the lower wall. On the other hand, numerous laboratory experiments and numerical simulations studying free mixing layers (that is, a step of infinite height) have been carried out. We consider then another configuration with a higher step ($W/H=1.25$), and compare the resulting structures with those obtained in free shear flows. The number of grid points is now $130\times40\times25$. The structure-function model is used to parametrize the subgrid scales. As opposed to the previous case, periodicity is assumed in the spanwise direction. Figure 7 shows the vorticity field at $t=138H/U_0$. Five primary rollers are present in the channel. As compared with Fig. 5, they are much less three dimensional, but exhibit spanwise oscillations, as other plots show. The third roller downstream from the step results from a pairing, which seems to occur in a quasi-two-dimensional fashion. The strain

FIG. 6. Top view of the isobar $p'=-0.3U_0^2/\rho_0$, in the same calculation as in Fig. 5.

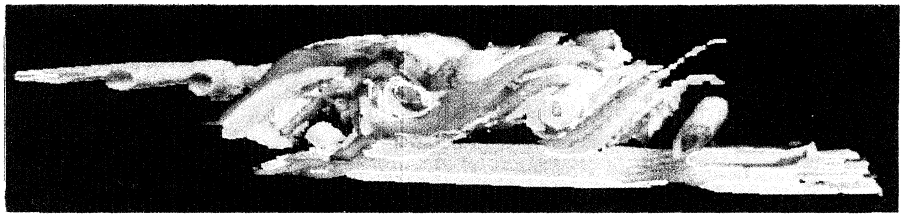

FIG. 7. Vorticity contours at time $t=138H/U_0$: blue, vorticity modulus $||\mathbf{w}||=1.8U_0/H$; green, streamwise vorticity $w_x=0.8U_0/H$ (aspect ratio $W/H=1.25$).

field induced by two consecutive Kelvin-Helmholtz vortices leads to the formation of streamwise vortices stretched along the braids. The ratio between their spanwise spacing and the local vorticity thickness is in good agreement with laboratory observations[13] (0.7 against 0.8). Figure 8 shows a cross section (in the y-z plane) of the longitudinal vortices through the braid between the second and the third Kelvin-Helmholtz vortices. It clearly shows counter-rotating vortices with a mushroomlike shape. These are analogous to the structures observed in laboratory experiments (Bernal and Roshko,[13] see their Fig. 12, and Lasheras and Choi[14]) and in direct numerical simulations[15] of free shear layers.

These new results concerning an inhomogeneous turbulent shear flow demonstrate the potentialities of a large-eddy simulation carried out with a finite-volume method (TRIO code) and a recently proposed subgrid model. In the two different geometries considered, the numerical simulations compare favorably with experiments, even for the detailed topology of the flow.

This study also shows the similarity of the flow downstream of a backward-facing step with the free mixing layer.

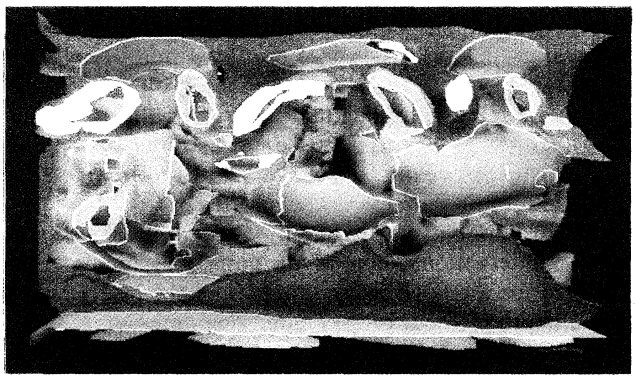

FIG. 8. Same calculation as in Fig. 7. Cross section of the longitudinal vortices: yellow, streamwise vorticity $w_x=+0.8U_0/H$; white, $w_x=-0.8U_0/H$.

The authors are indebted to the staff of LPML for developing the TRIO code, and to Y. Fouillet and E. David for their assistance in the visualizations. A.S.N. worked under a grant from Conselho Nacional de Desenvolvimento Científico e Tecnológico (Brazil). The computations were supported by Commissariat à l'Energie Atomique. Institut de Mécanique de Grenoble is sponsored by CNRS, Institut National Polytechnique de Grenoble, and Université Joseph Fourier.

[1]P. Moin and J. Kim, J. Fluid Mech. **118**, 341–377 (1982).

[2]H. Schmidt and U. Schumann, J. Fluid Mech. **200**, 511–562 (1989).

[3]J. K. Eaton and J. P. Johnston, Stanford University Report No. MD-39, 1980 (unpublished).

[4]A. Silveira Neto, D. Grand, and M. Lesieur, Int. J. Heat Mass Transfer (to be published).

[5]J. C. Buell and P. Huerre, in *Proceedings of the 1988 Summer Program* (Stanford University Report No. CTR-S88, 1988), pp. 19–27.

[6]F. W. Harlow and A. A. Amsden, J. Comput. Phys. 8, 197–213 (1971).

[7]P. H. Gaskell and A. K. C. Lau, Int. J. Numer. Methods Fluids **8**, 617–641 (1988).

[8]R. H. Kraichnan, J. Atmos. Sci. **33**, 1521–1536 (1976).

[9]J. P. Chollet and M. Lesieur, J. Atmos. Sci. **38**, 2747–2757 (1981).

[10]O. Métais and M. Lesieur, "Spectral Large-Eddy Simulation of Isotropic and Stable-Stratified Turbulence" (to be published).

[11]G. K. Batchelor, *The Theory of Homogeneous Turbulence* (Cambridge Univ. Press, Cambridge, 1953).

[12]J. Smagorinsky, Mon. Weather Rev. **91**, 99–164 (1963).

[13]L. P. Bernal and A. Roshko, J. Fluid Mech. **170**, 499–525 (1986).

[14]J. C. Lasheras and H. Choi, J. Fluid Mech. **189**, 53–86 (1988).

[15]R. W. Metcalfe, S. A. Orzag, M. E. Brachet, S. Menon, and J. J. Riley, J. Fluid Mech. **184**, 207–243 (1987).

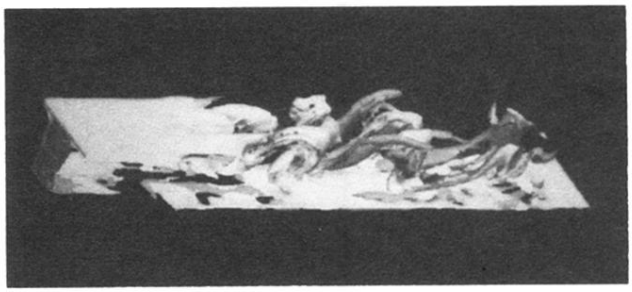

FIG. 5. Vorticity contours at time $t = 90H/U_0$: light gray, vorticity modulus $||\mathbf{w}|| = 3.5U_0/H$; dark gray, streamwise vorticity $w_x = 2.5U_0/H$ (aspect ratio $W/H = 2.5$).

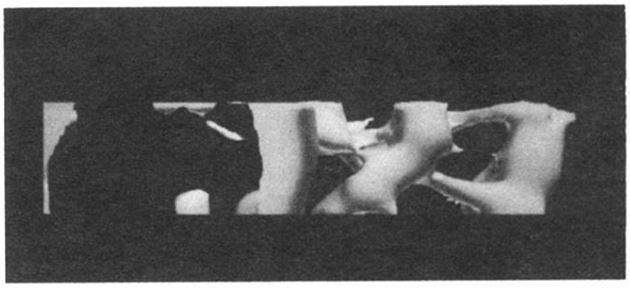

FIG. 6. Top view of the isobar $p' = -0.3U_0^2/\rho_0$, in the same calculation as in Fig. 5.

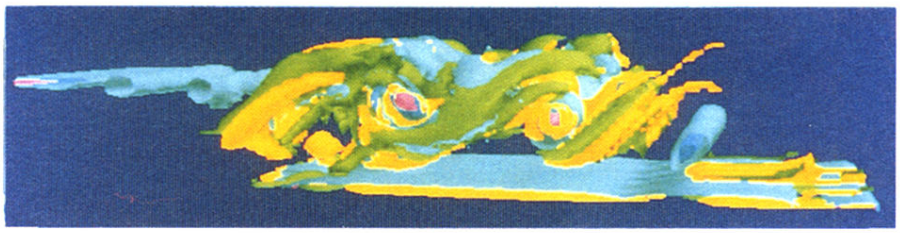

FIG. 7. Vorticity contours at time $t=138H/U_0$: blue, vorticity modulus $||\mathbf{w}||=1.8U_0/H$; green, streamwise vorticity $w_x=0.8U_0/H$ (aspect ratio $W/H=1.25$).

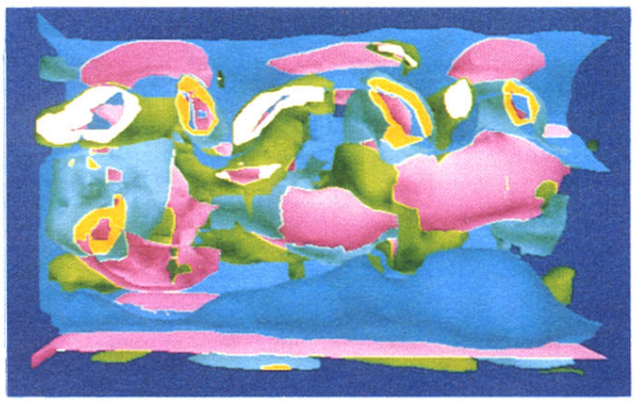

FIG. 8. Same calculation as in Fig. 7. Cross section of the longitudinal vortices: yellow, streamwise vorticity $w_x = +0.8U_0/H$; white, $w_x = -0.8U_0/H$.